Journal of Applied Polymer Science

Manipulation of the drug-release behavior of poly(glycolide-*co*-trimethylene carbonate)

Argyrios N. Nochos,[1,2] Konstantinos S. Andrikopoulos,[1,3] George A. Voyiatzis[1]

[1]Foundation for Research and Technology Hellas, Institute of Chemical Engineering Sciences (FORTH-ICE/HT), P.O. Box 1414 GR-26504 Rio-Patras, Greece

[2]Department of Pharmacy, University of Patras, GR-26504 Patras, Greece

[3]Department of Materials Science, School of Natural Sciences, University of Patras, GR-26504 Patras, Greece

Correspondence to: G. A. Voyiatzis (E-mail: gvog@iceht.forth.gr)

ABSTRACT: The current work focuses on Maxon, a modern biocompatible/bioabsorbable polymer, utilized in the fabrication of surgical sutures, and attempts to explore the limits of controlling the administration rate of a properly incorporated model drug, mitoxandrone dihydrochloride. The control is attempted by tailoring both the structural properties of the host polymer, more specifically its crystallinity and anisotropy, and the level of drug dispersion achieved after following different incorporation methods such as melt and dissolution mixing. The results, based on optical and electron microscopy, differential scanning calorimetry, Fourier transform infrared spectroscopy, and UV–vis spectroscopy, indicate that the structural parameters invoked may enable fine-tuning of the drug dose released within a 60-day period. Additionally, the burst effect of the active agent at the early stages of release is regulated by adjusting the drug dispersion level. © 2016 Wiley Periodicals, Inc. J. Appl. Polym. Sci. **2016**, *133*, 43915.

KEYWORDS: biomaterials; crystallization; degradation; drug delivery systems; films

Received 16 December 2015; accepted 8 May 2016

DOI: 10.1002/app.43915

INTRODUCTION

Biodegradable polymeric implants, such as surgical sutures, have been used for decades. However, their potential to be used as controlled drug delivery systems was realized only recently with the commercial release of Vicryl Plus[1] in 2004. Vicryl Plus is a synthetic absorbable suture composed of a glycolide/L-lactide copolymer coated with triclosan, an antibacterial agent. Since then, numerous research studies[2–5] have attempted to endow modern medical fibers with bioactive properties.

Polyglycolide (PGA) was the material chosen for the first synthetic absorbable suture commercialized in the 1970s under the name Dexon (Sherwood–Davis & Geck).[6] Beyond its commercial success, PGA is plagued by a rapid loss of its initial mechanical properties, which limits its medical applications; in two weeks its mechanical strength decreases by ~70%, while total absorption takes about 90 days.[7] Moreover, being a hard material compels its fabrication into a multifilament fiber, which in turn presents other disadvantages, such as tissue drag and an increased chance of harboring bacteria.[8] In an attempt to eliminate the above drawbacks, most of the new-generation synthetic absorbable sutures are based on copolymers of PGA with other monomers such as lactide and trimethylene carbonate (TMC), each one endowing the final material with different properties. Maxon, introduced in 1985, is nowadays one of the most popular of these materials. Structurally, it is a triblock copolymer ABA prepared by the ring-opening polymerization of glycolide (GA) and TMC with a final weight ratio of 0.675:0.325. There are two Maxon forms available: "Maxon B," where the (A) blocks are composed of PGA and the middle (B) segment is pure TMC, and "suture-based Maxon," where again the end blocks of the copolymer are PGA but the middle segment (B) is formed as a random copolymer of GA and TMC monomers. Suture-based Maxon, which is the material used in the present study, offers a much slower biodegradation rate (180–210 days) and is softer than PGA, allowing monofilament fibers to be fabricated. Moreover, the material is sterile, inert, and noncollagenous, has a high initial tensile strength, and offers greater knot security than polydioxanone, polyglactin, and polyglycolide.[6,8,9]

The hydrolytic degradation of Maxon has been extensively studied,[6,9,10] revealing a three-stage mechanism.[9] In the initial stage (inactive period), the polymer shows minimal water hydration and mass loss. Moving past the 20 days and into the second stage (active period), the water uptake increases and pores develop until the final postactive period (beyond 60 days in degradation media), where the polymer has reached a high

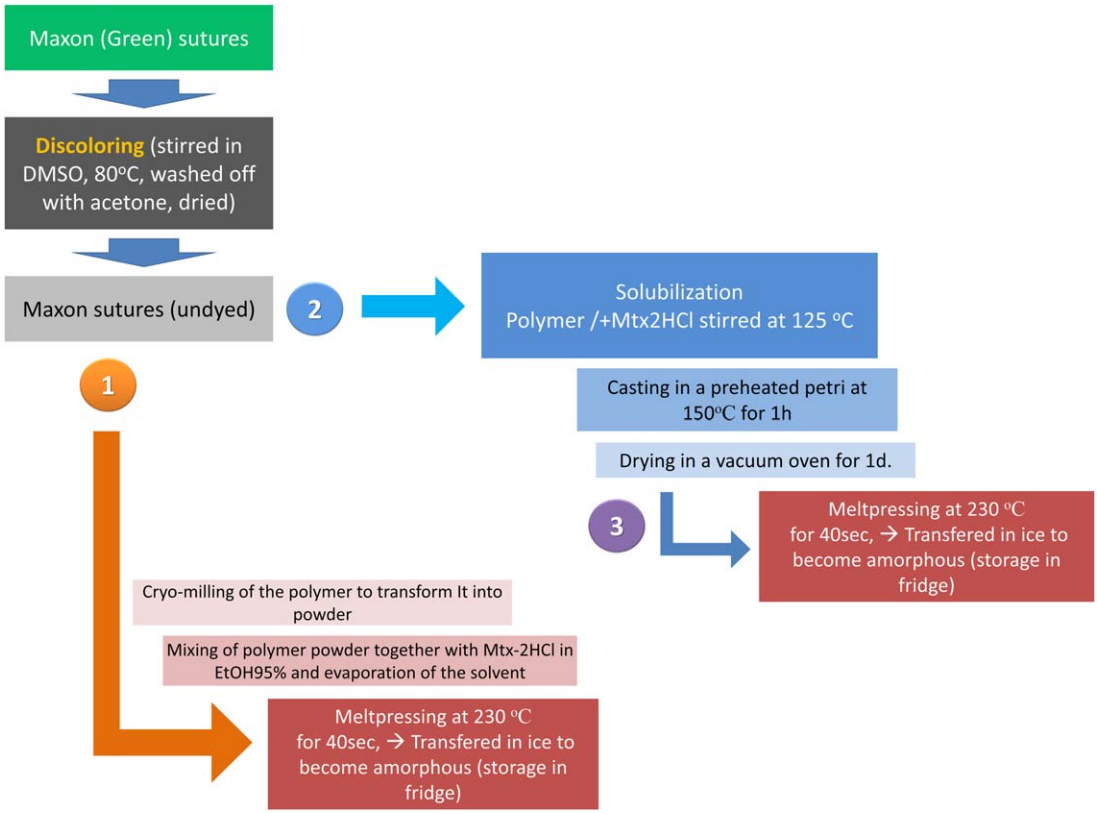

Figure 1. Descriptive illustration of all three sample preparation techniques. [Color figure can be viewed in the online issue, which is available at wileyonlinelibrary.com.]

hydration state and exhibits large cracks. A relevant study by Zurita *et al.*[6] has shown that the first stage of Maxon erosion can be associated with the hydrolysis of the soft segments (middle blocks). However, because of their insolubility, even the smallest degradation fragments of the copolymer remain entrapped in the matrix, accelerating the erosion process via an autocatalytic mechanism.

The prospect of using a Maxon suture as a controlled-release vehicle has to our knowledge been studied only by Noorsal *et al.*[9] Theophyline and sulfadiazine, two low-molecular-weight substances, were used as model drugs and were mixed with the polymer under melt conditions (melt compression). The release profiles of the drugs were not linear, and, according to the researchers, the loaded agent at the first stages of the polymer hydration was released mostly by diffusion, while in the later stages the degradation of the matrix was greatly involved. Despite the fact that the work of Noorsal *et al.* was particularly systematic, it did not suggest ways to actually control or simply prolong the release rate of the entrapped agent. However, regulation of the dosage of the drug that is administered by escaping the polymer carrier is of critical importance for medical applications.

A variety of drugs could be potentially loaded into fibers or small implants based on Maxon, producing bioactive surgical sutures or other multifunctional medical devices. Incorporating nonsteroidal anti-inflammatory drugs (NSAIDS) and local anesthetics may help in pain relief; antibiotics could protect the wound against infections, while anticancer drugs could help eradicate remnant cancer cells after a tumor-removal operation. Moreover, by controlling the release rate of the active agent and delivering it right onto the wound area may help eliminate toxicity effects, thus establishing a very effective drug-delivery system.

In some of our earlier studies,[11,12] we introduced the controlled implementation of anisotropy as a method to regulate the release rate of low-molecular-weight substances entrapped in semicrystalline polymers. We have shown that the introduction of anisotropy in high-density polyethylene samples leads to a reduction in the release rates measured in the case of triclosan incorporated into the polymeric matrix. A similar behavior was observed in the case of ibuprofen incorporated into a polypropylene matrix. The above deceleration effect on the drug release was attributed to a combination of increased polymer network density and crystallinity but also an improved drug dispersion induced through uniaxial stretching.

The present study investigates the means of controlling the release rate of a low-molecular-weight active agent incorporated in Maxon without chemical modification of the copolymer or the application of coatings. More particularly, mitoxantrone dihydrocloride, an antitumor drug, was loaded into Maxon films by both solvent dissolution and melt techniques, and then parameters such as drug distribution, polymer crystallinity, and macromolecular chain orientation achieved by uniaxial drawing were investigated for a possible impact on matrix degradation and drug-release properties.

Table I. Samples and Descriptions

Sample name	MTX %	Preparation method[a]	Treatment time at 75 °C	Draw ratio, λ
SC	1	SC	0 min	1
SC-MP_A	1	SC-MP	0 min	1
SC-MP_C	1	SC-MP	24 h	1
SC-MP_C_Dr	1	SC-MP	24 h	2.5
MP_C	1	MP	24 h	1
MP_C_Dr	1	MP	24 h	2.5

[a] SC, solvent casting; MP, melt pressing; SC-MP, solvent casting with subsequent melt pressing.

EXPERIMENTAL

Materials

In agreement with a number of research works that investigate suture-based drug-delivery systems, we preferred to use real surgical fibers instead of lab-synthesized polymers.[4,9,13,14] Maxon sutures (Syneture, 6307-71, monofilament, size 1) were purchased from eSutures.com, Mokena, Illinois. Mitoxantrone dihydrochloride (MTX) was purchased from Santa Cruz Biotechnology, Dallas, Texas. Phosphate buffer saline (PBS) solution was synthesized according to Ref.[15]. Dimethyl sulfoxide (DMSO), acetone, and ethanol 95% were purchased from Sigma-Aldrich, Taufkirchen, Germany.

Dye-Removal Process

The green dye existing in the original sutures was removed in order to minimize its interference in the UV–vis spectral range used for the quantification of the migrated drug. Maxon sutures cut into small pieces (<1 cm) were undyed by stirring into a DMSO solution at 80 °C, where the material shows a swelling effect. The solvent was replaced three times, and the final colorless suture fibers were washed with acetone and dried for several days in a vacuum oven at 100 °C in order to remove any solvent remnants. The dye-removal process followed here is comparable to the ones used in other articles.[13,14]

Drug-Incorporation Methods

For the incorporation of MTX in Maxon, three different methodologies were followed (summarized in Figure 1) and are described in detail in the subsequent paragraphs.

Thermal Method: Melt Pressing (MP). Undyed sutures cut in pieces were pulverized using a cryogenic impact mill (Freezer/Mill 6750, SPEX SamplePrep, Metuchen, New Jersey). Powdered polymer was mechanically mixed with fine-grained MTX, and the admixture was immersed and stirred in ethanol 95% (where only the drug is partly soluble) until the solvent evaporated. The resulting mixture was then pressed in a heated hydraulic press at 230 °C with a pressure of 2 MPa (30 s preheat and 10 s pressing) and was immediately placed on ice in order to inhibit crystallization. The process results in uniform semitransparent beige films with a thickness of ~130 μm.

It must be mentioned that, according to the literature,[16] MTX does not decompose until 250 °C; thus the drug load is considered to be intact after the MP process.

Solubilization Method: Solvent Casting (SC). Known quantities of precut sutures together with MTX were stirred in DMSO at 125 °C for 10 min (the total ratio of solid to solvent was always kept at 1 g per 14 mL of DMSO in order to preserve the viscosity of the solution). The solution was rapidly transferred into a petri dish preheated in an oven at 150 °C and kept there for 1 h and subsequently the oven was deactivated and the sample was left to cool slowly at room temperature. The film was finally dried in a vacuum oven at 70 °C for an extra day. Because of their excessive porosity (see the scanning electron microscopy images in the Results and Discussion section) and their degraded mechanical properties, all films created by this method were not thoroughly studied.

Combined Method (Solvent Casting + Melt Pressing, SC-MP). In order to eliminate the porosity and consequently the thermal history of the films, the previously solvent-cast samples were pressed in a hot press following the relevant process described in the thermal method.

Sample Records

All of the samples used in the present study are recorded in Table I along with their preparation method, their properties, and the name that will be used from now on to describe them. Several parameters were considered in order to study their influence on the drug-release and polymer-degradation properties; namely drug distribution, the percentage of polymer crystallinity (see next section), and the draw ratio λ.

Crystallinity Variation

The modification of crystallinity was achieved by thermal treatment of the polymer films at their crystallization temperature T_c (75 °C measured by differential scanning calorimetry) for different time intervals up to 1 day (Table I). Treated samples were stored at 4 °C until use to inhibit any extra crystallization development.

Uniaxial Drawing

Selected dumbbell-shaped test strips (SC-MP_C_Dr and MP_C_Dr) with a narrow midsection of 6.5 mm width and 57 mm length (type II, norm ASTM D 638) were cut from ~130 μm thick films and subsequently uniaxially stretched in a homemade stretching element[17] at room temperature at a draw rate of 3 cm/min. The draw ratio, λ, has been preset, and it is defined as the ratio of the extended length to the original length determined from the displacement of ink marks on the film strip cut from the narrow midsection of the dumbbell-shaped test strip.

Morphological Study: Optical and Electron Microscopy

For the morphological study of the films, we utilized an optical microscope (Leica DM 2500M, Buffalo Grove, Illinois) with polarizing filters and an attached digital camera (DFC420 C). In addition, scanning electron microscope images were collected using a Zeiss SUPRA 35VP system, Jena, Germany.

Thermal Properties and Crystallinity

The thermal properties of the films were studied by differential scanning calorimetry (DSC), utilizing the Q100 (TA Instruments, New Castle, Delaware) model equipped with a controllable cooling system. The samples weighing 6–12 mg were encased in

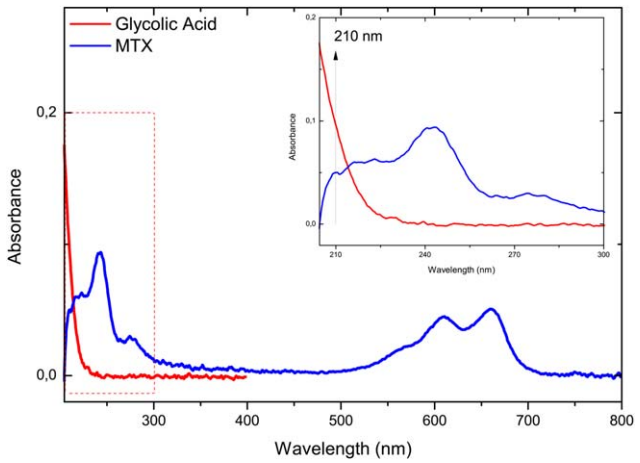

Figure 2. UV–vis absorbance spectra of glycolic acid and MTX in a PBS (pH 7.4) solution. The inset depicts a magnification of the low-wavelength spectral region. [Color figure can be viewed in the online issue, which is available at wileyonlinelibrary.com.]

aluminum caps, and the system was calibrated with indium. The temperature range 0–220 °C was scanned at a rate of 10 °C/min. The percentage of crystallinity $\%X_c$ of a polymer sample was calculated by the equation

$$\%X_c = \frac{\Delta H_m - \Delta H_c}{\Delta HF_o} \times 100 \quad (1)$$

where ΔH_m and ΔH_c are the melting and crystallization enthalpies, respectively. Furthermore, since only the A (PGA) blocks of the Maxon copolymer contribute to the crystallinity of the sample, we consider ΔHF_o the enthalpy of fusion of a perfect PGA polymer crystal (139.1 J/g).[16]

Degradation Studies

Two methods were used to study the decomposition of Maxon: Fourier transform infrared spectroscopy with attenuated total reflection (FTIR-ATR) and UV–vis spectroscopy. The samples studied in both methods were placed in vials containing a PBS solution and remained under constant stirring (100 rpm) at 37 °C for about 60 days (a C24 incubator, classic series, New Brunswick Scientific, Hamburg, Germany was utilized for the temperature control and stirring). PBS is often used as a release medium because it resembles blood in values of pH, osmotic concentration, and concentration of ions.

For the application of the first method (FTIR-ATR), parts of the PBS immersed samples were cut at predetermined time intervals, wiped gently with a paper towel to remove surface water droplets, and dried for 8 h in a vacuum oven at room temperature. Spectra from the dried films were then collected via an ATR accessory (MIRacle, Pike Technologies, Madison, Wisconsin) in a Bruker FRA104 FTIR spectrophotometer, Billerica, Massachusetts in order to record changes in their structure that are attributed to erosion.

In the second method (UV–vis absorption), instead of the polymer films themselves, their decomposition media were examined for the presence of glycolic acid monomers (or oligomers) that are released as the matrix erodes. About 1.5 mL from each solution was removed, measured in a UV–vis spectrophotometer (Hitachi U-3000, Schaumburg, Ilinois), and returned back to its vial.

As seen in Figure 2, the glycolic acid shows an absorption peak at wavelengths lower than 200 nm, but because of instrumental limitations only part of it is visible. Using prototype solutions, a calibration curve of the absorbance of glycolic acid at 210 nm (the high-wavelength wing of its absorption band) as a function of concentration was extracted. From the latter, the concentration of glycolic acid in the released media was calculated after subtraction of the MTX contribution in the same spectral range (calculated by taking into account the respective absorbance at 660 nm).

Estimation of Molecular Orientation

Polarized FTIR-ATR spectra were utilized in order to estimate the induction of molecular orientation of the drawn samples. A KRS-5 wire-grid polarizer, Barrington, New Jersey was positioned before the sample to set the incident polarization of the infrared radiation. The sample in examination was rotated by 90° so that dichroic measurements parallel and perpendicular to the draw-axis geometry could be acquired. The molecular orientation was estimated by the calculation of the IR dichroism as well as the second moment of the orientation distribution function, P_2.

Release Studies

The UV–vis absortion spectra of the immersed drug-loaded samples were collected in a manner similar to the method used to study the decomposition rate described above. Using an appropriate calibration curve, the absorbance values at 660 nm were transformed into concentration values of MTX.

RESULTS AND DISCUSSION

Uniaxial Drawing

The amorphous Maxon material, similar to the one produced after quenching it from the melt in ice, exhibits mechanical properties analogous to the ones described by rubber elasticity. Thus, when a uniaxially stretched amorphous Maxon sample is released from the grabs of the drawing device, it returns very

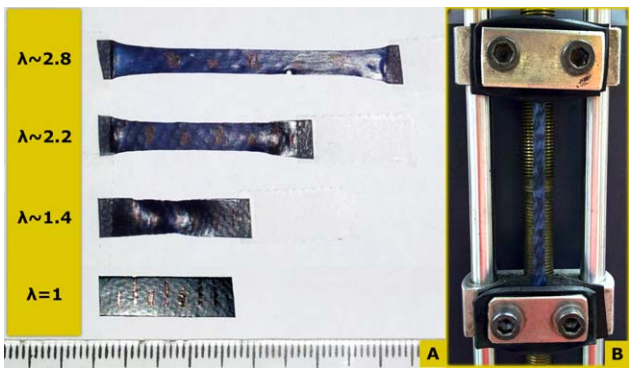

Figure 3. Images of (A) Maxon SC-MP_C samples (thermally treated for 1 day at 75 °C) drawn at various draw ratios and (B) a sample of the same batch drawn at $\lambda \sim 4$ held at the grabs of the stretching device. [Color figure can be viewed in the online issue, which is available at wileyonlinelibrary.com.]

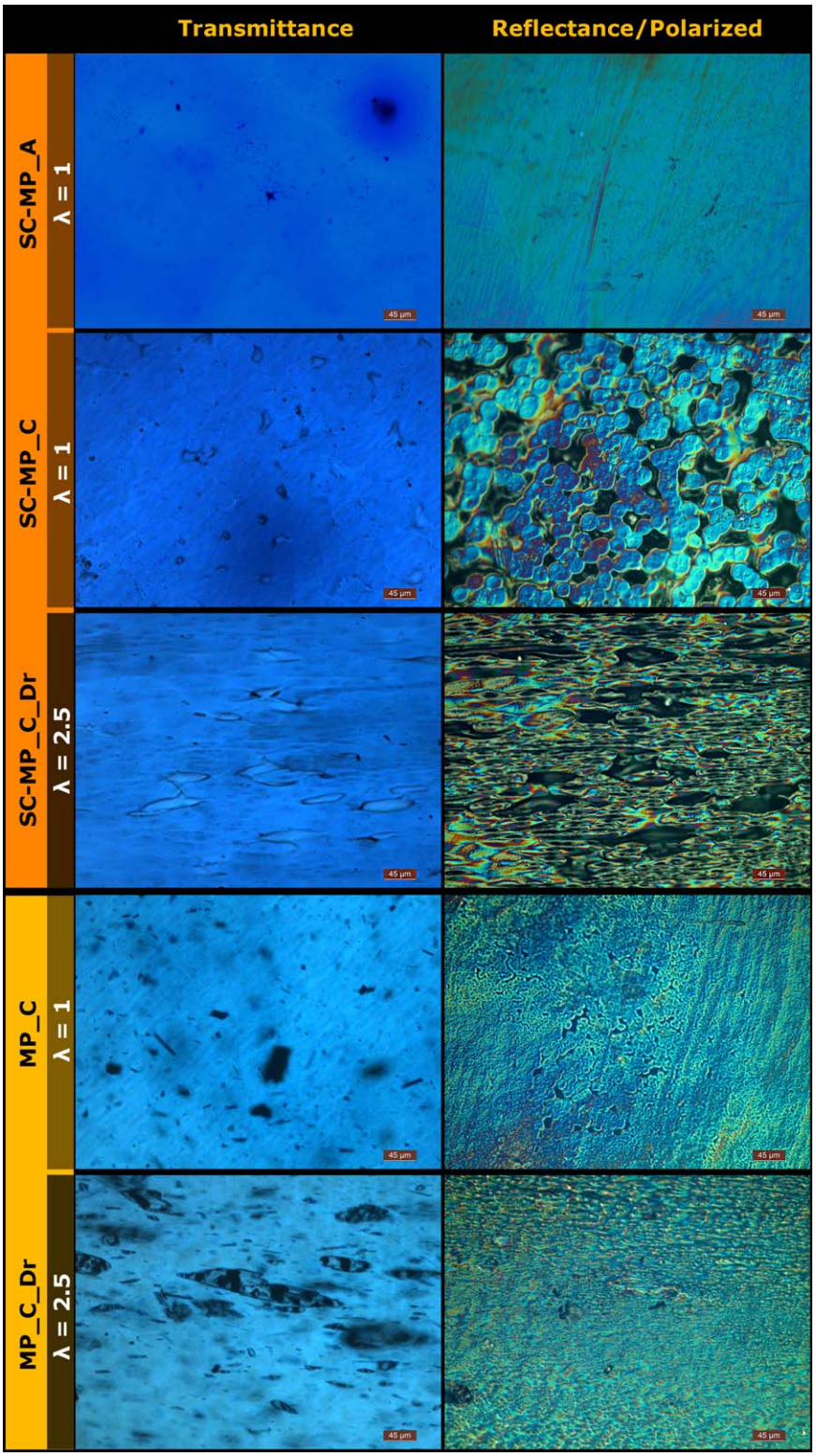

Figure 4. Polarized optical microscopy images in transmittance (left column) and reflectance (right column) configurations of the samples SC-MP_A (first row), SC-MP_C (second row), SC-MP_C_Dr (third row), MP_C (fourth row), and MP_C_Dr (fifth row). [Color figure can be viewed in the online issue, which is available at wileyonlinelibrary.com.]

promptly almost to its original size. Only the films created by the SC-MP or MP methods that were subsequently treated at 75 °C for 24 h could retain part of their drawn length in the form of a plastic deformation. For these samples, therefore, a possibility of retaining some degree of molecular orientation attained during stretching exists, and thus these are the samples

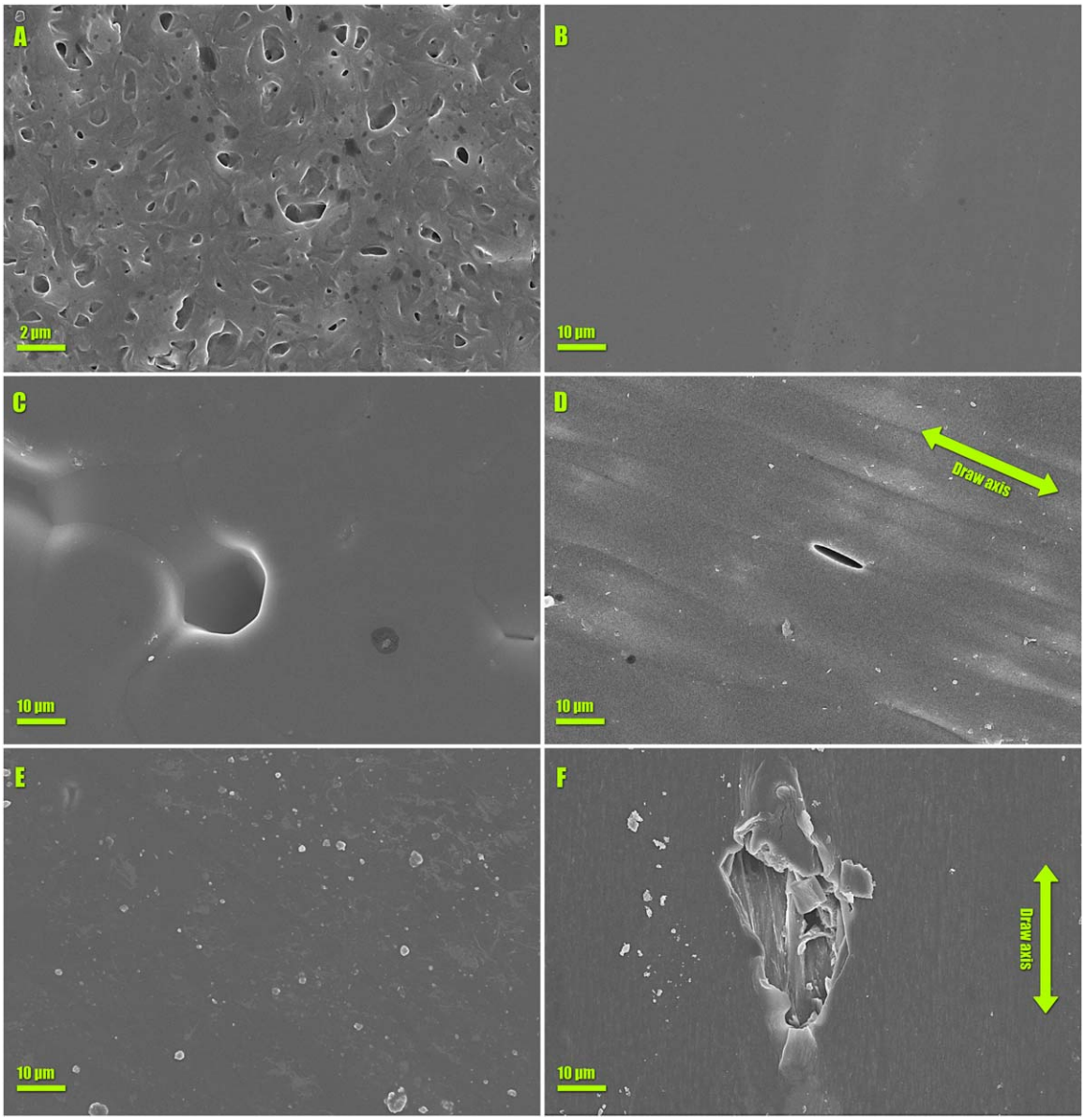

Figure 5. SEM images of samples (A) SC, (B) SC-MP_A, (C) SC-MP_C, (D) SC-MP_C_Dr, (E) MP_C, and (F) MP_C_Dr. [Color figure can be viewed in the online issue, which is available at wileyonlinelibrary.com.]

studied thoroughly in the current work. Figure 3 shows images of Maxon samples (SC-MP, crystallized at 75 °C for 24 h) uniaxially stretched at room temperature at different draw ratios. The blue color is characteristic of MTX incorporated in the films at 1 wt %. The longest draw ratio, λ, achieved was $\lambda = 4$. However, after being released from the holders, the sample relaxed to $\lambda \sim 3$. During the drawing process, white stripes evolve in the sample [Figure 3(B)] above $\lambda \sim 3$, which continue to grow until they cover its entire surface. These opaque stripes are attributed to the induced crystallization upon stretching, which creates microstructures that scatter the visible light.

Morphological Study

Figure 4 shows representative optical microscopy images from the examined samples acquired in polarized transmittance and reflectance configurations. By comparing the SC-MP_A film with the thermally treated SC-MP_C (Figure 4, first and second rows, respectively), it is clear that crystallites 15–30 μm in size (reflectance images) have developed on the latter. In contrast, in its amorphous counterpart, no such structures are observed. Moreover, the uniform deep-blue color of the SC-MP films (in transmission images), typical of MTX, suggests the good dispersion of the drug into the polymer matrix with only scarce distinct particles visible.

Moving on to the MP samples, examination of the transmittance micrographs (Figure 4, last two rows) reveals large particles of the drug (up to 50 μm), while at the same time they lack the deep-blue saturation previously reported in SC-MP films (which is considered a sign of optimal MTX dispersion in the polymer matrix). Investigating the microstructure of uniaxially drawn samples, it is apparent that spherulites in both SC-

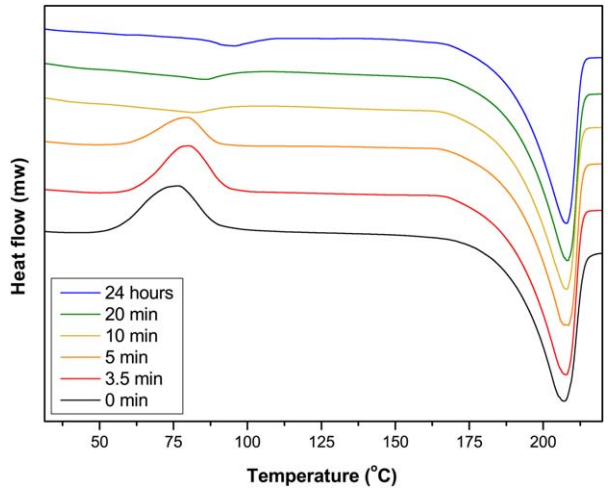

Figure 6. Thermograms of SC-MP films thermally treated for different times at 75 °C. [Color figure can be viewed in the online issue, which is available at wileyonlinelibrary.com.]

MP_C_Dr and MP_C_Dr film batches (Figure 4, rows 3 and 5, respectively) have been transformed into "needle"-like structures. Furthermore, the spherulites of the MP films are much smaller in diameter than those of the SC-MP batch, probably due to confinement by the large drug crystals present. Finally, in the spots where drug particles were placed in the isotropic MP film, pores seem to be generated during drawing.

Scanning electron micrographs of the main samples are presented in Figure 5 and offer a more detailed examination of the film surfaces. The extreme porosity of the solvent-cast Maxon films as depicted in Figure 5(A) degraded the mechanical properties of those samples to the point that their uniaxial stretching was impossible. For this reason, we decided to abandon that preparation technique in favor of a combined method that incorporates a final melt-pressing step, as described previously. On the other hand, the thus-formed SC-MP films [Figure 5(B,C)] exhibited a much smoother surface. Confirming the optical microscopy results, the melt-pressed samples [Figure 5(E)] showed a lower dispersion of MTX in the polymer with drug particles visible on the film surface, in contrast with the SC-MP samples, where no such crystals were observed. Moreover, during the stretching of the film, the large drug crystals dispersed in it induce cavities in the vicinity of their location that may allow the entry of the solvent. In contrast, in the SC-MP samples the drug is considered to be dispersed at a molecular level.

Thermal Properties and Crystallinity

Figure 6 compares the thermograms from SC-MP Maxon-MTX films thermally treated at the polymer's crystallization temperature ($T_c = 75$ °C) for different time intervals (0–24 h). The crystallization and melt transitions are visible at ~75 °C and 213 °C, respectively. It is clear that as the treatment time increases, the exothermic crystallization peak decreases, and it completely disappears after the exposure at T_c for more than 10 min. By measuring the melt and crystallization enthalpies (ΔH_m and ΔH_c, respectively), we calculated [via eq. 1] the increase in the percentage of crystallinity $\%X_c$ and plotted it against time of thermal treatment in Figure 7(a). The thermal crystallization at T_c occurred quite abruptly: 30 min of exposure was enough for the polymer to reach an apparent maximum of crystallinity (32.8%). From the thermally treated samples, the most crystalline ($t = 1$ day) and the most amorphous one, from now on referred to as SC-MP_C and SC-MP_A, respectively, were selected to further investigate differentiations in their drug-release and degradation kinetics.

Polymer crystallinity was also calculated for the SC-MP_C uniaxially drawn films, and the results are presented in Figure 7(b). Just like the optical observations suggested (see Figure 4, third row), DSC measurements confirmed that drawn samples exhibit

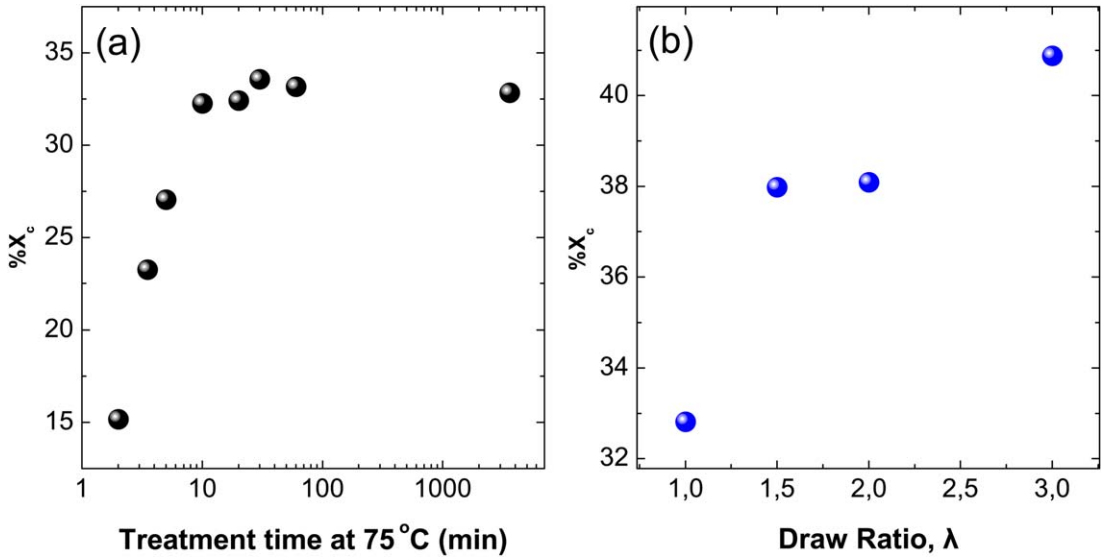

Figure 7. (a) Percentage of polymer crystallinity ($\%X_c$) of SC-MP films plotted versus time of thermal treatment at 75 °C. (b) Percentage of polymer crystallinity ($\%X_c$) of SC-MP_C films (previously treated for 1 day at 75 °C) versus draw ratio λ. [Color figure can be viewed in the online issue, which is available at wileyonlinelibrary.com.]

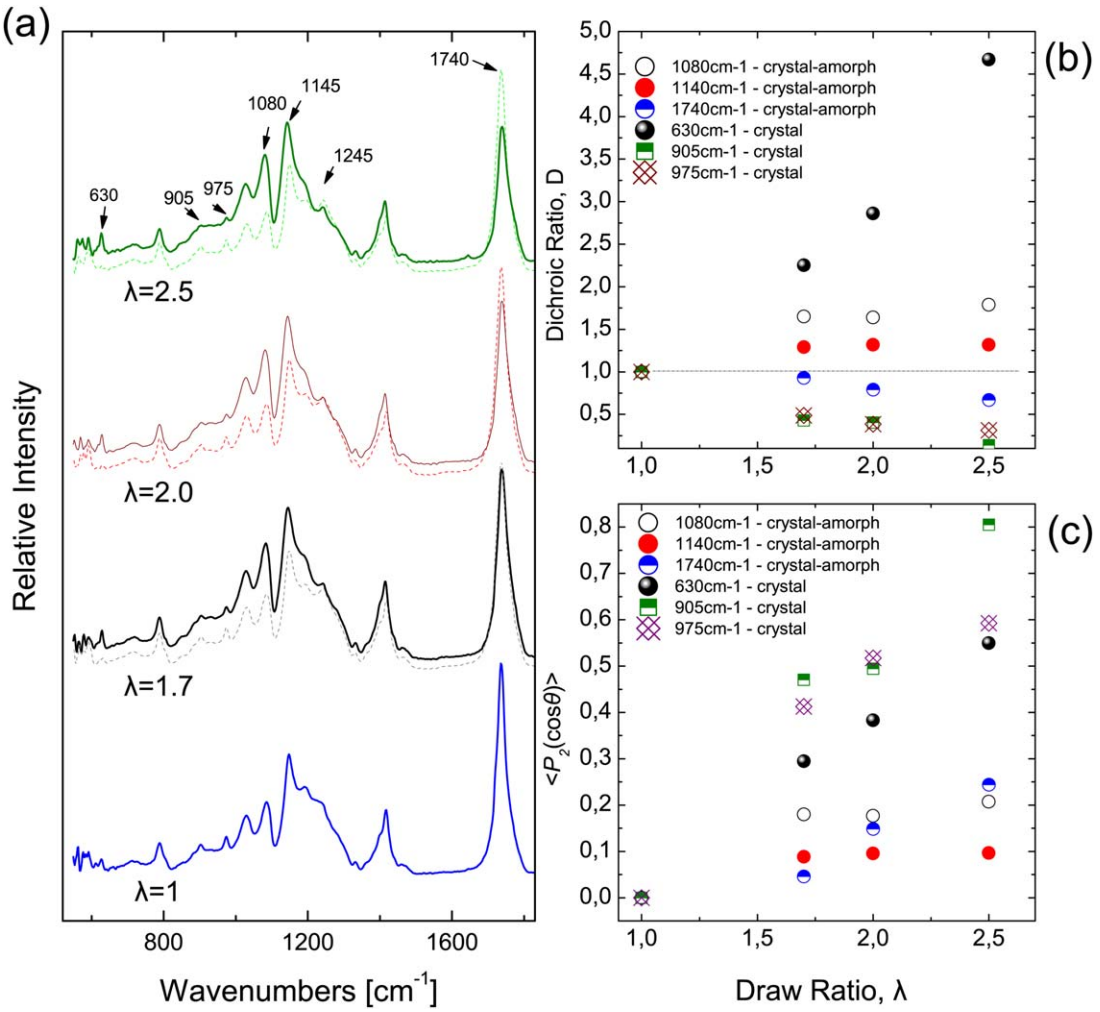

Figure 8. (a) Polarized FTIR-ATR spectra of SC-MP_C samples uniaxially drawn at various draw ratios λ. The spectra have been vertically shifted to facilitate their comparison. Presented with dashed and continuous lines are the spectra acquired perpendicular and parallel to the draw-axis polarization geometry, respectively. For $\lambda = 1$ the sample is isotropic. (b) Dichroic ratio, *D*, for select vibrational peaks of Maxon. (c) Second moment of the orientation distribution function for selected vibrational modes as a function of draw ratio. [Color figure can be viewed in the online issue, which is available at wileyonlinelibrary.com.]

a draw-induced crystallization that increases with the draw ratio. More specifically, the $\%X_c$ increased from 32.8% in the isotropic (unstretched, $\lambda = 1$) film up to 40.9% for the higher draw ratio attained ($\lambda = 3$).

Molecular Orientation Estimation

The structure of the untreated films was studied by FTIR spectroscopy, which additionally enabled the anisotropy evaluation of the stretched samples.

Figure 8(a) depicts polarized FTIR-ATR spectra of a series of SC-MP_C samples stretched at various draw ratios (up to $\lambda = 2.5$, sample SC-MP_C_Dr). In the same figure, a spectrum of an unstretched (isotropic) sample is also given. The main absorption bands of Maxon are clearly observed in all spectra and are summarized in Table II.

The anisotropy of the series of uniaxially stretched samples was characterized by the calculation of the dichroic ratio, *D*, defined as the absorbance ratio for a selected vibrational band when using two different polarizations of the incident infrared radiation that are mutually perpendicular:

$$D = \frac{A_{\parallel}}{A_{\perp}} \tag{2}$$

where $A_{\parallel}$ and $A_{\perp}$ are the absorbance for infrared radiation polarized parallel and vertical to the draw axis, respectively.

The dichroic ratio of most of the Maxon vibrational bands [Figure 8(b)] changes progressively with the draw ratio, either increasing or decreasing, depending on the angle α formed by the dipole moment derivative vector of each vibrational band with respect to the vector associated with the orientation of the polymeric segment. This progressive alteration of the dichroic ratio indicates a corresponding gradual development of segmental orientation. It is known that *D* assumes values < 1 for vibrational modes possessing dipole moment derivatives that tend to be perpendicular to the macromolecular chains (e.g., C═O stretching band at 1740 cm^{-1}). In contrast, "skeletal" vibrations, vibrational modes possessing dipole moment derivatives that

Table II. Assignment of the Major Vibrational Bands of Maxon and the Associated Dichroic Ratio Trend for Anisotropic Samples

Band frequency (cm^{-1})	Assignment	Structure	Dichroic ratio, *D*
630	C=O deformation	Crystalline PGA	>1 (significant increase)
720	C=O deformation	Mostly amorphous	~1
905	νC—C+rCH_2	Crystalline PGA	<1 (significant decrease)
975	νC—C+rCH_2	Crystalline PGA	<1 (significant decrease)
1030	ν_sCOC	Mostly TMC amorphous	>1
1080	ν_sCOC	Crystalline/amorphous PGA	>1 (shallow increase)
1140	ν_{as}COC	Mostly crystalline PGA	>1 (shallow increase)
1415	CH_2 bending	Crystalline PGA	~1
1740	νC=O	Crystalline/amorphous PGA	<1 (shallow decrease)

are almost parallel to the macromolecular chain (e.g., C—O—C stretching at 1080 cm^{-1}), assume *D* values > 1 as λ increases. If the angle α is known, we may extract the second-order Legendre polynomial, P_2, of the expansion of the orientation distribution function in related series:

$$P_2 = \frac{D-1}{D+2} \cdot \frac{2}{3\cos^2 a - 1} \quad (3)$$

The P_2 values for the 630 cm^{-1}, 1080 cm^{-1}, and 1140 cm^{-1} bands and the 905 cm^{-1} , 975 cm^{-1}, and 1740 cm^{-1} bands are calculated under the assumption that $\alpha \approx 0°$ and $\alpha \approx 90°$, respectively, and are plotted as a function of draw ratio in Figure 8(c). Bands assigned to neat amorphous or mixed amorphous/crystalline regions are characterized by low P_2 values, in contrast to neat crystalline regions, which exhibit relatively higher P_2 values.

Degradation and Hydrolysis

The hydrolysis of the Maxon matrix for the structurally different samples under investigation was studied by both direct and indirect measurements. The first type of measurement involved the films' structural characterization as a function of time by accumulation of IR spectra, while the second type involved the monitoring of the release of glycolic acid monomers as well as the respective oligomers (GA) into the solvent as a function of time by UV–vis experiments.

Structural Characterization of the Hydrolyzed Films. Puiggali and coworkers[18–21] have performed extensive studies on the characterization of PGA/TMC copolymers by several techniques, including FTIR spectroscopy. Our band assignment, discussed in the previous section, is mostly based on their reports. Their particularly comprehensive work on the characterization of the copolymer's crystallinity as well as the characterization of the TMC concentration by FTIR spectroscopy may be used in order to explore the structure of the hydrolyzed films under investigation. According to Puiggali, the ratio of the integrated intensity of the 630 cm^{-1} band to the respective sum of the intensities of the 630 cm^{-1} and 720 cm^{-1} bands is proportional to the crystallinity of the copolymer. Figure 9(a) depicts this ratio as a function of hydrolysis time for three samples: the mostly

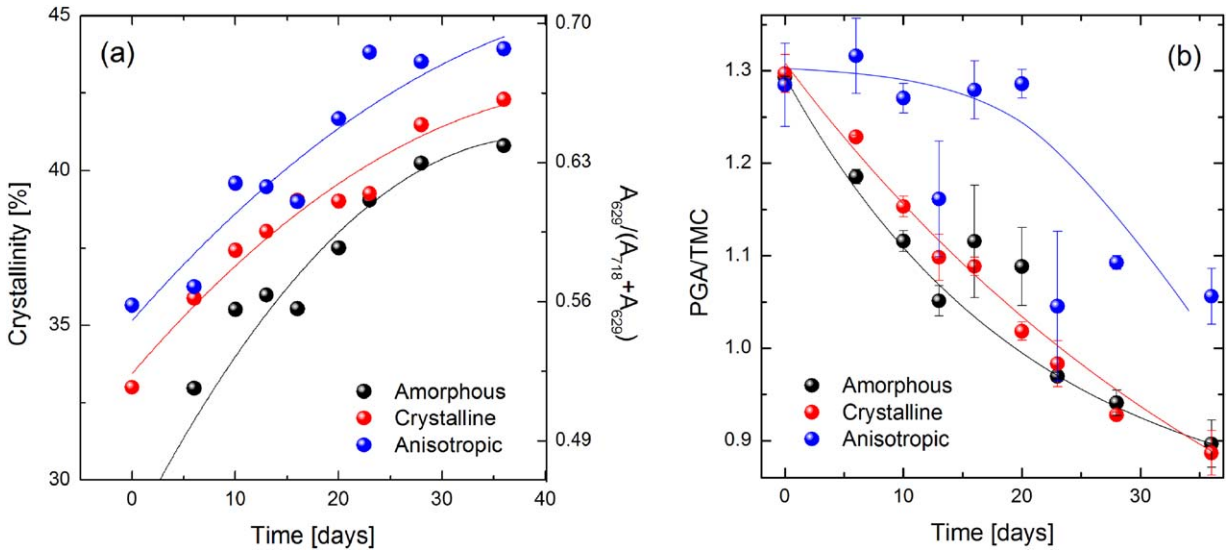

Figure 9. The evolution of (a) crystallinity for the almost amorphous sample (SC-MP_A), the sample possessing the highest crystallinity (SC-MP_C), and the anisotropic sample (SC-MP_C_Dr) and (b) the PGA/TMC ratio for the same samples as a function of hydrolysis time. [Color figure can be viewed in the online issue, which is available at wileyonlinelibrary.com.]

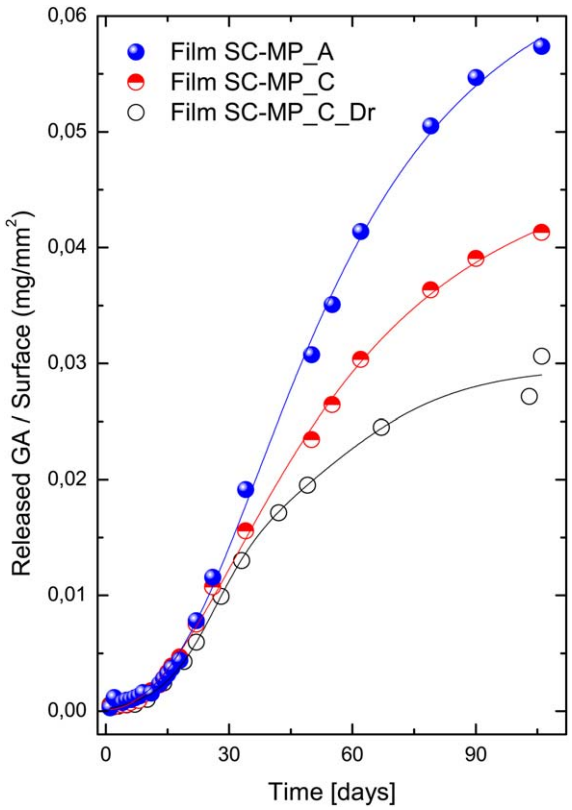

Figure 10. Cumulative release of glycolic acid monomer normalized by surface as a function of time for the amorphous (SC-MP_A), crystalline (SC-MP_C), and uniaxially drawn crystalline (SC-MP_C_Dr) film samples. [Color figure can be viewed in the online issue, which is available at wileyonlinelibrary.com.]

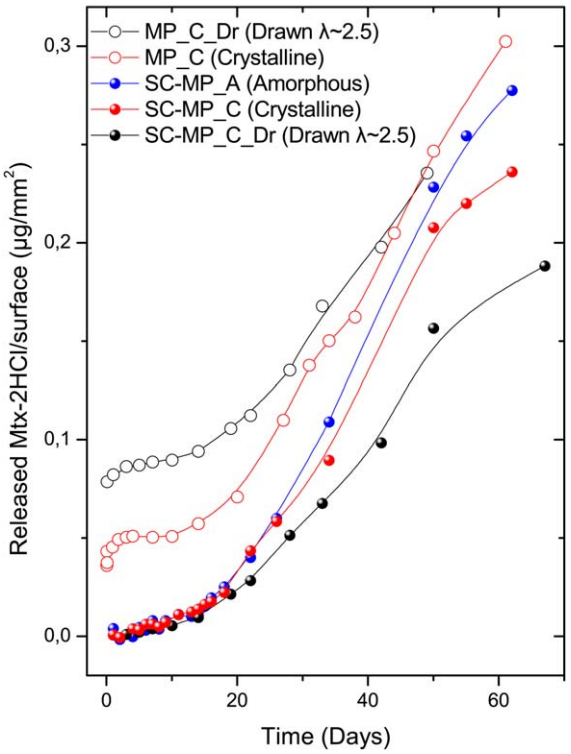

Figure 11. Cumulative release of MTX normalized by surface as a function of time for various samples. [Color figure can be viewed in the online issue, which is available at wileyonlinelibrary.com.]

amorphous one (SC-MP_A), the sample with the maximum thermally induced crystallinity (SC-MP_C), and the anisotropic sample (SC-MP_C_Dr). Taking into account that the crystallinity of the SC-MP_C sample is known by the DSC experiments, we corresponded the crystallinity of this particular sample to the mentioned intensity ratio. The latter enabled the estimation of the crystallinity of all samples during their exposure to hydrolysis from their respective FTIR spectra. The crystallinity of all films exhibits a significant increase during the hydrolysis time. This increase may be explained by the fact that hydrolysis proceeds within the amorphous phase of the material. The mostly amorphous film crystallizes quickly during the treatment period, and, at ~40 days, its crystallinity almost reaches that of sample SC-MP_C at the same treatment time. The integrated intensity ratio of the 1080 cm^{-1} and 1030 cm^{-1} bands is proportional to the PGA and TMC fragments in the sample. A plot of this ratio as a function of hydrolysis treatment time is shown in Figure 9(b). Hydrolysis causes scission of the polymeric chains, and the resulting fragments migrate into the solvent; thus, it is evident that all investigated samples become richer in TMC as hydrolysis proceeds. However, the PGA content decrease is different for each of the samples. The most prominent decrease is exhibited by the SC-MP_A sample, while the SC-MP_C sample demonstrates a slightly slower reduction. Sample SC-MP_C_Dr shows a different behavior, with a shallow decrease during the first 20 days, followed by a reduction comparable to one of the two previously mentioned samples.

Direct Monitoring of GA. The cumulative release profiles of GA divided by film surface for samples of varying crystallinity (SC-MP_A, SC-MP_C, and SC-MP_C_Dr) are presented in Figure 10. The profiles seem to be partitioned into two separate stages, in agreement with previous studies on Maxon degradation.[6,9] At the first stage, from zero to about 18 days, the release of GA is minimal, and all three profiles seem to be identical. According to the literature,[6] in this stage mainly the soft amorphous segments of the material decompose together with some defective crystalline regions because they are less dense and are more accessible to the water structure. However, the majority of oligomers and even a population of monomers fail to escape from the dense polymer matrix and trigger an autocatalytic hydrolysis effect by reacting with the polymer chains. This behavior explains the nonlinearity of the GA release profiles. Advancing to the next stage, which begins after day 19, the release profiles start to diverge increasingly with time. The release of the GA at this stage is much higher but also seems to be inversely proportional to the polymer crystallinity as the amorphous sample SC-MP_A seems to degrade faster than the thermally treated one, SC-MP_C, and the latter is faster than the annealed-drawn one, SC-MP_C_Dr. This behavior could be attributed to the decreased penetration of water into the denser, highly packed crystalline regions that are abundant in the thermally treated samples. Moreover, it is possible that in the

oriented samples oligomers are more efficiently trapped in the tighter matrix created during uniaxial stretching, while simultaneously the accommodation of water is limited.

Release Studies

Figure 11 compares the release profiles of MTX for the case of the amorphous, crystalline, and uniaxially stretched crystalline Maxon films prepared by the solvent-casting and melt-pressing (SC-MP) and melt-pressing (MP) methods. The overall shape of the SC-MP release curves is analogous to the one shown by Noorsal *et al.*,[9] being partitioned into two distinct stages and similar to the release of GA examined in the previous paragraph. In the first step of the profiles (0–18 days), the escape of the MTX seems to be minimal, and the three profiles almost match. In the second stage, which starts after day 19, the release of the active agent has significantly increased, and the profiles of the three samples start to deviate, with the less crystalline unloading more drug. Noorsal and his research group have suggested that in the initial stage the release of the drug is controlled by diffusion, while at the second step polymer hydrolysis plays a vital role. As expected, our results seem to agree that the films exhibiting a faster degradation rate also showed a stronger release of the loaded active agent. Thus, if compared with the SC-MP_C_Dr sample, the total quantity of the released drug at the end of the 60th day for the SC-MP_C and SC-MP_A samples is higher by ~33% and ~55%, respectively. This effect could be attributed to the decreased penetration of water in more crystalline polymer matrices; this is further diminished in the oriented polymer materials.

An interesting release behavior is the one exhibited by the MP samples where the drug dispersion in the polymer matrix is particularly low. More specifically, a burst effect is observed at the early stages of the release for both isotropic and stretched samples. This is attributed to the large (micron-scale) particles of MTX present in the polymer (Figure 4, row 4), which generate pores or cavities during stretching [as seen in the SEM image, Figure 5(F)]. The burst effect is more prominent for the drawn samples, an observation that may be explained by the existence of pores that can easily expose the near-surface drug crystals to the solvent, solubilizing them instantly. In summary, the two-stage release mechanism applies also for the MP samples; however, the first stage is dominated by the burst effect, which is more intense for the drawn samples. The second stage is similar to the one exhibited by the SC-MP samples: the release rate of the drawn sample is lower than that of the isotropic sample (the induced crystallinity or molecular orientation effect dominates the release), and at ~50 days, an intersection of the release curves is observed.

CONCLUSIONS

Maxon was successfully used as a drug-release vehicle for low-molecular-weight drugs, such as mitoxantrone dihydrochloride. Modifiable physical properties of the polymer matrix, such as the percentage of polymer crystallinity and the molecular orientation (sample anisotropy), were found to enable the fine-tuning of the release rate of the incorporated drug and therefore control the dosage administered via a medical implant in a real-life scenario. The same properties showed a measurable impact on the polymer degradation or erosion; thus, the samples having higher crystallinity and particularly the anisotropic ones exhibited increased resistance to degradation. Furthermore, the dispersion of the drug in the polymeric matrix was proved to play a crucial role in its early-phase release, especially in the case of the anisotropic samples. Of the two polymer–drug mixing techniques we studied, solvent dissolution can be considered as the most efficient, reaching a level of dispersion close to molecular. The melt mixing technique, on the other hand, resulted in the existence of relatively large drug particles within the polymer matrix. As vividly demonstrated by optical and electronic microscopy, the presence of these poorly dispersed drug microparticles led to the formation of stretch-induced pores on the uniaxially drawn samples, which in turn caused a burst release effect in the early release time intervals. Depending on the drug and its targeted purpose, this may be useful for some applications (e.g., topical anesthetics) or should be completely avoided in others (e.g., toxic antitumor agents).

In summary, modification of a film's crystallinity or anisotropy (within the studied limits) enabled the control of the drug release up until day 60 by a factor of two, while modification of the drug's dispersion in the polymeric matrix enabled the control of early drug release by at least two orders of magnitude. It is anticipated that the control of the drug released at the later stages may be further affected in the case of samples possessing optimum drug dispersion and higher anisotropy than the ones studied in the current work.

The outcomes of this research work may be useful for future studies related to the creation of bioactive sutures or similar drug-loaded implants with slow-release and erosion properties. Such systems may be suitable for the controlled release of highly toxic drugs or applications demanding an extended treatment period.

ACKNOWLEDGMENTS

This research has been cofinanced by the European Union (European Social Fund) and Greek national funds through the Operational Program "Education and Lifelong Learning" of the National Strategic Reference Framework (NSRF) Research Funding Program: Heracleitus II (12/119/5).

REFERENCES

1. Ethicon, History of Innovation; http://www.ethiconproducts.co.uk/about/ethicon-history/ethicon-innovations (Accessed Dec. 2, 2015).
2. Zhukovskii, V. A. *Fibre Chem.* **1996**, *28*, 369.
3. Blaker, J. J.; Nazhat, S. N.; Boccaccini, A. R. *Biomaterials* **2004**, *25*, 1319.
4. Zurita, R.; Puiggalí, J.; Rodríguez-Galán, A. *Macromol. Biosci.* **2006**, *6*, 767.
5. Wang, L.; Chen, D.; Sun. J. *Langmuir* **2009**, *25*, 7990.
6. Zurita, R.; Franco, L.; Puiggalí, J.; Rodríguez-Galán, A. *Polym. Degrad. Stabil.* **2007**, *92*, 975.
7. King, M. W.; Chung, S. In Biomaterials Science, 3rd ed.; Buddy, D.; Ratner, B. D.; Hoffman, A. S.; Schoen, F. J.; Lemons, J. E.,

Eds.; Academic Press: Cambridge, Massachusetts, **2013**; Chapter I.2.14, pp 301–320.

8. Franco, L.; Bedorin, S.; Puiggalí, J. *J. Appl. Polym. Sci.* **2007**, *104*, 3539.
9. Noorsal, K.; Mantle, M. D.; Gladden, L. F.; Cameron, R. E. *J. Appl. Polym. Sci.* **2005**, *95*, 475.
10. Díaz-Celorio, E.; Franco, L.; Rodríguez-Galán, A.; Puiggalí, J. *Polym. Degrad. Stabil.* **2010**, *95*, 2376.
11. Iconomopoulou, S. M.; Voyiatzis, G. A. *J. Controlled Release* **2005**, *103*, 451.
12. Nochos, A. N.; Kontoyannis, C.; Voyiatzis, G. A. *Macromol. Symp.* **2013**, *331–332*, 115.
13. Zhang, X.; Thomas, V.; Vohra, Y. K. *J. Biomed. Mater. Res., Part B* **2009**, *89B*, 135.
14. Blanco, M. G.; Franco, L.; Puiggalí, J.; Rodríguez-Galán, A. *J. Appl. Polym. Sci.* **2009**, *114*, 3440.
15. Cold Spring Harbor Protocols, Phosphate-buffered Saline (PBS); http://cshprotocols.cshlp.org/content/2006/1/pdb.rec8247 (Accessed Dec. 2, 2015).
16. American Home Products Corporation, Wyeth-Ayerst. Novantrone Material Safety Data Sheet; http://www.amatheon.com/msds/Novantrone_Wyeth.pdf (Accessed Dec. 2, 2015).
17. Voyiatzis, G. A.; Andrikopoulos, K. S. *Appl. Spectrosc.* **2002**, *56*, 528.
18. Márquez, Y.; Franco, L.; Turon, P.; Rodríguez-Galán, A.; Puiggalí, J. *Polym. Degrad. Stabil.* **2013**, *98*, 2709.
19. Díaz-Celorio, E.; Franco, L.; Puiggalí, J. *J. Appl. Polym. Sci.* **2010**, *116*, 577.
20. Díaz-Celorio, E.; Franco, L.; Rodríguez-Galán, A.; Puiggalí, J. *Eur. Polym. J.* **2012**, *48*, 60.
21. Díaz-Celorio, E.; Franco, L.; Rodríguez-Galán, A.; Puiggalí, J. *Polym. Degrad. Stabil.* **2013**, *98*, 133.